View metadata, citation and similar papers at core.ac.uk

brought to you by CORE

provided by CiteSeerX

Linköping University Post Print

CrNx Films Prepared by DC Magnetron Sputtering and High-Power Pulsed Magnetron Sputtering: A Comparative Study

Grzegorz Greczynski, Jens Jensen and Lars Hultman

N.B.: When citing this work, cite the original article.

©2010 IEEE. Personal use of this material is permitted. However, permission to reprint/republish this material for advertising or promotional purposes or for creating new collective works for resale or redistribution to servers or lists, or to reuse any copyrighted component of this work in other works must be obtained from the IEEE.

Grzegorz Greczynski, Jens Jensen and Lars Hultman, CrNx Films Prepared by DC Magnetron Sputtering and High-Power Pulsed Magnetron Sputtering: A Comparative Study, 2010, IEEE TRANSACTIONS ON PLASMA SCIENCE, (38), 11, 3046-3056.
http://dx.doi.org/10.1109/TPS.2010.2071885
Postprint available at: Linköping University Electronic Press
http://urn.kb.se/resolve?urn=urn:nbn:se:liu:diva-63154

CrN_x Films Prepared by DC Magnetron Sputtering and High-Power Pulsed Magnetron Sputtering: A Comparative Study

Grzegorz Greczynski, Jens Jensen, and Lars Hultman

***Abstract*—CrN_x $(0 \leq x \leq 0.91)$ films synthesized using high-power pulsed magnetron sputtering, also known as high-power impulse magnetron sputtering (HiPIMS), have been compared with those made by conventional direct-current (dc) magnetron sputtering (DCMS) operated at the same average power. The HiPIMS deposition rate relative to the DCMS rate was found to decrease linearly with increasing emission strength from the Cr ions relative to Cr neutrals, in agreement with the predictions of the target-pathway model. The low deposition rate in HiPIMS is thus a direct consequence of the high ionization level ($\sim$56%) of the target material and effective capturing of Cr ions by the cathode potential. Although the HiPIMS deposition rate did not exceed 40% of the DCMS rate, the drop in the relative deposition rate upon increasing the N_2-to-Ar flow ratio, $f_{N_2/Ar}$, was found to be similar for both sputtering techniques. Films prepared by HiPIMS contained similar amounts of atomic nitrogen as the dc-sputtered samples grown at the same $f_{N_2/Ar}$, indicating that the nitride formation at the substrate takes place mostly during the time period of the high-power pulses, and the N_2 uptake between the pulses is negligible. The microstructure evolution in the two types of CrN_x films, however, differed clearly from each other. A combination of a high substrate bias and a high flux of doubly charged Cr ions present during the HiPIMS discharge led to a disruption of the grain growth and renucleation, which resulted in column-free films with nanosized grains not observed in the conventional DCMS-based process. The comparison of nanoindentation hardness as a function of $f_{N_2/Ar}$ revealed superior properties of HiPIMS-sputtered films in the entire range of gas compositions.**

***Index Terms*—CrN, high-power impulse magnetron sputtering (HiPIMS), high-power pulsed magnetron sputtering, magnetron sputtering.**

I. Introduction

MAGNETRON sputtering is a commonly used technique for production of various types of thin-film coatings for a wide range of industrial applications. In the conventional direct-current (dc) magnetron sputtering (DCMS), the power density on the cathode is typically several watts per square centimeter, resulting in plasma densities on the order of $\sim 10^{17}$ m^{-3}. Under these conditions, the ionized fraction of the sputter-ejected material usually does not exceed a few percent [1], [2]; as a consequence, majority of film-forming species arrive at the substrates as neutrals with an energy described by the Sigmund–Thompson distribution function [3], [4]. Much effort has been made over the years to increase the degree of ionization of the sputtered material in order to allow for a control of both the energy and the trajectory of film-forming species [5]. One of the more recent developments in this area is high-power pulsed magnetron sputtering, which is also known as high-power impulse magnetron sputtering (HiPIMS), where the idea of increasing the degree of ionization by means of increasing the temporal plasma density in front of the sputtering target has been utilized [6]. An increase in the plasma density (in some cases, exceeding 10^{19} m^{-3} [7]) is achieved by applying high-power pulses (several watts per square centimeter, $\sim$100 μs) with a low duty factor (a few percent) in order to keep the average power on the level typical for conventional dc sputtering (limited by the thermal load of the target). The resulting ionization of the sputtered flux shows high dependence on the target material [8] in all reported cases, which is significantly higher than for DCMS performed under similar conditions. The downside of the high ionization achieved in HiPIMS plasmas is the apparent drop in the deposition rate compared with DCMS at the corresponding power level [9]. Numerous possible scenarios have been put forward to explain this issue [10]–[15], and it becomes clear that the physical phenomena that account for the rate loss may depend not only on the choice of processing gas and target material but also on detailed arrangement of the sputtering system. Since high deposition rates are crucial for most of the industrial applications, substantial effort [16], [17] is being made to resolve this issue.

Until now, HiPIMS has also been used in reactive mode to deposit a number of industrially attractive coatings [18]–[29], often with promising properties not achievable by other sputtering techniques. In particular, several researchers have studied HiPIMS-grown CrN films [18], [19], [21] as well as CrN-based multilayer films [22], [26]. Ehiasarian *et al.* [21] have grown CrN_x films from a circular Cr target (50-mm diameter) on steel substrates at self-bias and heated up to 250 °C for N_2-to-Ar partial pressure ratios varied between one and five. The obtained films were droplet-free and exhibited defect-free dense columnar structure. Excellent adhesion, hardness, corrosion, and wear resistance were also reported. In the next paper by the same group [18], one of the films (N_2-to-Ar partial pressure ratio of four) was compared with a single-layer CrN and

Manuscript received February 8, 2010; revised May 11, 2010 and June 29, 2010; accepted August 4, 2010. Date of publication September 27, 2010; date of current version November 10, 2010. This work was supported by the European Research Council (ERC) Advanced Grant.

The authors are with the Thin Film Physics Division, Department of Physics (IFM), Linköping University, 581 83 Linköping, Sweden.

Digital Object Identifier 10.1109/TPS.2010.2071885

0093-3813/$26.00 © 2010 IEEE

multilayer superlattice CrN/NbN coatings deposited by the arc-bond sputtering (ABS) technique [30]. The process parameters in the latter case were however quite different (200 × 600 mm targets, N_2-to-Ar partial pressure ratio of one, bias voltage between -75 and -100 V, and substrate temperature of 400 °C). Nevertheless, the CrN films prepared by HiPIMS showed, in this comparison, a wear resistance and adhesion properties comparable with those of the superlattice CrN/NbN coatings produced by the state-of-the-art ABS technology. Alami *et al.* [19] have studied CrN films prepared by HiPIMS at constant N_2 flow for different values of the peak target current and compared results with a reference dc-sputtered film. The authors reported morphology change from columnar to featureless as the amplitude of the peak target current was increased and no effect on the film density and surface roughness. It is not clear, however, what was the effect of the pulsing frequency that was varied at the same time on the microstructure of the resulting films.

CrN_x films were also grown by modulated pulse power (MPP) sputtering (a modification of HiPIMS) and compared with those obtained using DCMS and middle-frequency bipolar pulsed magnetron sputtering [29]. Using the same set of process parameters for all three methods, the authors were able to demonstrate superior properties of CrN films prepared by MPP-sputtering technique.

In order to increase the understanding of the benefits and drawbacks of a novel technology, CrN_x films with varying nitrogen content were synthesized using both HiPIMS and conventional DCMS sources by means of varying the N_2-to-Ar flow ratio. For a reliable comparison, all other process parameters, including substrate temperature, substrate bias, and the total gas pressure, were kept constant in both cases. The same, industry-scale sputtering target was also used for both HiPIMS and DCMS film growth. The microstructure and mechanical properties of the resulting films are analyzed and compared. Interpretation of the obtained results is performed with the help of optical emission spectroscopy and ion mass spectroscopy studies performed in parallel.

Of primary interest were questions not addressed in the previous studies. In particular, the relationship between the nitrogen content in the gas mixture and resulting film composition, microstructure, crystal phases, and mechanical properties was in focus. This is particularly interesting since, until now, very little is known about the nature of reactive HiPIMS. The disruptive character of the film-deposition process, where freshly deposited portion of the target species is exposed to the reactive gas mixture for milliseconds (long enough to allow for a potential compound formation) before the next high-power pulse, may, on its own (i.e., apart from other effects like those induced by the high ion content), affect the structure and properties of the resulting films.

II. Experimental Setup

All the films were grown in an industrial CC800/9 coating system manufactured by CemeCon AG in Germany. The relevant details of the system configuration can be found in [31]. A single rectangular Cr target of dimensions 88×500 mm^2 was sputtered in Ar/N_2 atmosphere in either HiPIMS or DCMS operational mode. For each experiment, the deposition process consisted of the following steps: 1) radiation heating (2-kW heating power for 30 min.); 2) radiation heating (0.5-kW heating power for 30 min.), resulting in a substrate temperature of $T_S \sim 200$ °C and background pressure on the order of 1–2 mPa; 3) deposition of a ~30-nm-thick Cr film in order to improve adhesion and reduce stress at the substrate interface (heating power kept at 0.5 kW); and 4) deposition of a CrN_x film at an average power of 4 kW (in the case of HiPIMS, the pulsing frequency was set to 300 Hz, resulting in energy per pulse $E_p = 13.3$ J). The cathode pulselength and the bias pulselength were both set to 200 μs. Under these experimental conditions, the peak target current varied between 380 and 500 A (increasing with increasing N_2 component in the gas mixture), whereas the negative peak target voltage was between 795 and 810 V. To facilitate comparison, all films (HiPIMS and dc-sputtered) were deposited at a constant average power of 4 kW and negative substrate bias voltage $V_S = 150$ V. The N_2-to-Ar flow ratio $f_{N_2/Ar}$ was varied between zero and two in order to investigate the effect of nitrogen partial pressure on the coating composition and microstructure. The total gas pressure during all depositions was kept constant at 0.4 Pa. Silicon wafers with native oxide layer were used as substrates. Prior to depositions, the substrates were ultrasonically cleaned in acetone and isopropanol. No substrate rotation was used during deposition; the substrate-to-target distance was ~7 cm. The Tektronix DPO4054 500-MHz-bandwidth digital oscilloscope was used to monitor and record the current and voltage transients during HiPIMS depositions.

The film composition was determined by the time-of-flight elastic recoil detection analysis (ToF-ERDA) at Uppsala University, Sweden, using a 40-MeV I^{9+} ion beam. Data were evaluated using the CONTES code [32]. Scanning electron microscopy (SEM) was carried out on cross sections of fractured films using the LEO 1550 Gemini scanning electron microscope. The crystal structure was determined by X-ray diffraction (XRD) with a Bruker AXS D8 Advance diffractometer operated in the $\theta-2\theta$ mode using Cu Kα radiation. The UMIS nanoindenter was used for the evaluation of mechanical properties of the as-deposited films. A minimum of 20 indents were performed on each sample with the maximum load set to 15 mN. The average hardness values were then extracted by the Oliver and Pharr method [33]. The resulting confidence intervals were higher than 93%.

The ion-energy distribution functions (IEDFs) were measured both in time-averaged and time-resolved mode with a PSM003 mass spectrometer from Hiden Analytical, U.K., as was described in [34]. The orifice of the spectrometer was grounded and aligned along the target-surface normal. Using the same settings (in order to enable relative ion-content estimates), the IEDFs for the following ions were measured: Ar^+, Ar^{2+}, Cr^+, Cr^{2+}, N_2^+, N^+, and CrN^+. The IEDFs were typically recorded for more than one isotope of a given ion in order to eliminate the risk of detector saturation. The inverse mass transmission function was applied to the raw data due to the fact that quadrupole mass analyzers are known to possess higher transmission at lower mass [35]. In order to facilitate

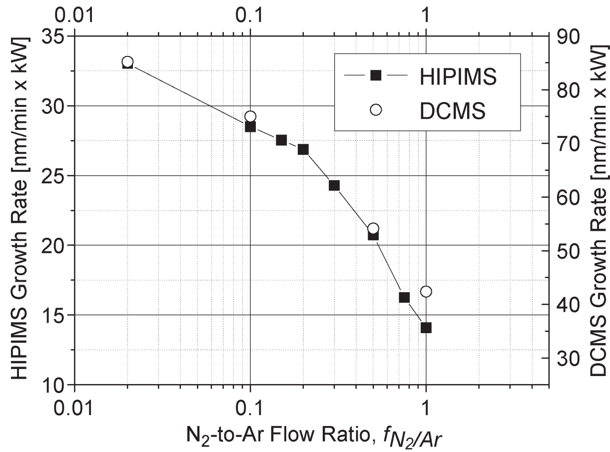

Fig. 1. Comparison between HiPIMS and conventional DCMS growth rates per kilowatt of the average power. The growth rate is plotted as a function of the N_2-to-Ar flow ratio $f_{N_2/Ar}$. Vertical axes are scaled in such way that the relative drop with respect to the metallic mode can also be compared between both sputtering techniques.

reliable plasma analysis with mass spectrometry, the cathode was dismounted from its original location (chamber door) and placed flat on the substrate table with the target facing upward. The distance between the target surface and the mass-spectrometer orifice was set to 21 cm. A Mechelle Sensicam 900 optical emission spectrometer connected to a collimator via an optical fiber was used to record the emission from the plasma. Data were recorded in a line-of-sight geometry with the probe placed outside the port window of the chamber and directed toward the racetrack. The spectral range of the spectrometer was 300–1100 nm, and its shutter speed was set to 100 ms, allowing for data averaging over multiple HiPIMS pulses. The measured line intensities were corrected for the transition probabilities and level degeneracy.

III. Results and Discussion

It has been recognized early that the benefits of HiPIMS in terms of high ionization of the target material come at the cost of a lowered deposition rate [36]–[38]. If referred to the conventional DCMS at the same average power, the time-averaged HiPIMS rate in most of the cases constitutes only a fraction of the DCMS rate [8], [9]. The physical reasons that may account for this behavior include the following: 1) the effective capturing of the ionized portion of the sputtered material as described by the target-pathway model [10], [11]; 2) the enhanced radial transport (across the magnetic-field lines) that increases deposition rates at the side of the cathode (perpendicular to the target surface) and decreases a fraction of sputtered materials reaching the substrate placed directly in front of the target [14]; 3) lower sputtering efficiency at higher target voltage typically used in HiPIMS that results from the fact that sputter yield increases with increasing ion energy that is less than in a linear way [15]; 4) changes in plasma impedance that may effectively reduce the voltage available for the sheath so that it constitutes a lower fraction of the total target voltage than it is the case with DCMS at the corresponding average power [12]; and 5) for some materials with low self-sputtering yield, a reduction in deposition rate may be observed

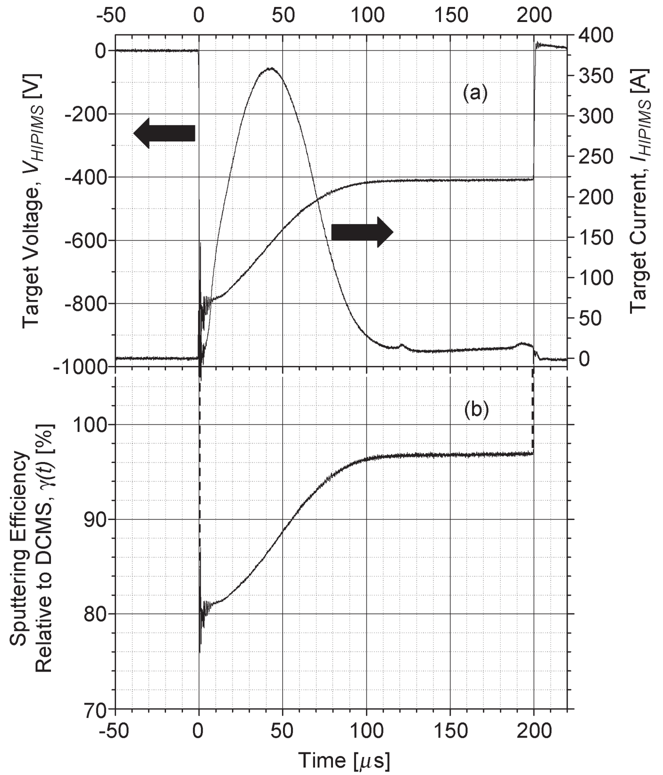

Fig. 2. (a) Target-current and target-voltage waveforms for $f_{N_2/Ar} = 0$ along with (b) the sputtering-efficiency function.

if the pulselength is long enough to allow for transition to the self-sputtering mode [12].

Fig. 1 shows the HiPIMS deposition rate as a function of the N_2-to-Ar ratio $f_{N_2/Ar}$ in comparison with the DCMS rate at the same average power of 4 kW. Depending on $f_{N_2/Ar}$, the HiPIMS rate constitutes between 40% ($f_{N_2/Ar} = 0$) and 33% ($f_{N_2/Ar} = 1$) of the DCMS rate, which corresponds well to the earlier results obtained on the laboratory-scale systems [8], [9]. As evident from the figure, the deposition rate decreases with increasing $f_{N_2/Ar}$ and at least two reasons can be identified that account for this behavior, namely: 1) nitride formation on the surface of the sputtering target (poisoning effect) and 2) lower sputtering efficiency of the N_2 gas with respect to Ar. It is interesting to note, however, that the relative drop in the deposition rate with increasing $f_{N_2/Ar}$ (with respect to the metallic mode of operation) is similar in the two sputtering techniques. In the case of DCMS, at $f_{N_2/Ar} = 1$, the rate drops to 49% of the value measured in the metallic mode ($f_{N_2/Ar} = 0$), while the corresponding number for HiPIMS is 43%. In order to explain the low deposition rates during HiPIMS processing in our system, we consider in more detail two effects: 1) less-effective sputtering due to higher target voltages used in HiPIMS as well as 2) the loss of material caused by the back attraction of Cr ions at the target. Potential influence of the other factors that were mentioned previously and that could also lead to lower rate is not treated here explicitly as there is no obvious way to quantify these effects.

In Fig. 2(a), the target-current and target-voltage waveforms during the HiPIMS discharge driven at an average power of 4 kW and $f_{N_2/Ar} = 0$ are shown. The 200-μs-long pulses can be seen as composed of the high-current phase (0–100 μs)

followed by the dc-like discharge (100–200 μs) as described elsewhere [39]. During the pulse, the negative target voltage $V_{\rm HiPIMS}(t)$ varies significantly (predominantly due to the limitations of the power supply), and its amplitude drops from the initial 800 to 400 V at the end of the high-current phase (100 μs). For comparison, with sputtering in the dc mode at the same average power, the target voltage $V_{\rm DC}$ is constant in time and amounts to 368 V ($f_{N_2/Ar} = 0$). Because the target voltage is significantly higher in the HiPIMS case, a certain drop in the sputtering efficiency (and, thus, deposition rate) is expected owing to the fact that the sputter yield does not increase linearly with increasing ion energy, as was pointed out by Emmerlich *et al.* [15]. To quantify this effect, we define the relative sputtering-efficiency function $\gamma(t)$ as

$$\gamma(t) = \frac{\beta(t)}{\alpha(t)} \times 100\% \tag{1}$$

where $\alpha(t)$ stands for the temporary ratio of $V_{\rm HiPIMS}(t)$ and $V_{\rm DC}$

$$\alpha(t) = \frac{V_{\rm HiPIMS}(t)}{V_{\rm DC}} \tag{2}$$

and $\beta(t)$ is the temporary ratio of HiPIMS ($Y_{\rm HiPIMS}$) and DCMS ($Y_{\rm DC}$) sputter yields

$$\beta(t) = \frac{Y_{\rm HiPIMS}\left(V_{\rm HiPIMS}(t)\right)}{Y_{\rm DC}(V_{\rm DC})}. \tag{3}$$

In the energy range of interest (300–800 eV),[1] the Ar^+ and Cr^+ sputter yields simulated using the TRIM software [40] are very similar, which greatly simplifies the treatment as the details of the transition from gas-dominated sputtering into the self-sputtering regime do not need to be considered in detail. Since the dependence of sputter yield on the target voltage in the aforementioned energy range can be fitted with a power function of the form

$$Y(V) = aV^b \tag{4}$$

we can express the HiPIMS and DCMS sputter yields as

$$Y_{\rm HiPIMS}(t) = aV^b_{\rm HiPIMS}(t) \tag{5}$$
$$Y_{\rm DC} = aV^b_{\rm DC}. \tag{6}$$

Finally, the HiPIMS-to-DCMS relative sputtering efficiency defined in (1) can be rewritten using (2) and (3), and (5) and (6) as

$$\gamma(t) = V^{1-b}_{\rm DC} V^{b-1}_{\rm HiPIMS}(t) \times 100\%. \tag{7}$$

Fig. 2(b) shows the relative sputtering-efficiency function for HiPIMS processing in metallic mode ($f_{N_2/Ar} = 0$).[2] In this case, $V_{\rm DC} = 368$ V, and the fitting of TRIM-simulated sputter yields accordingly with (4) gives the exponent $b = 0.7286$. As can be seen, the sputtering efficiency constitutes between 81%

[1] We neglect here the effect of multiply-charged ions; therefore, the ion energy of interest is given directly by the amplitude of the target voltage.

[2] Since target poisoning is expected to be different between HiPIMS and DCMS for a given $f_{N_2/Ar}$, analogical analysis for $f_{N_2/Ar} > 0$ is rather meaningless.

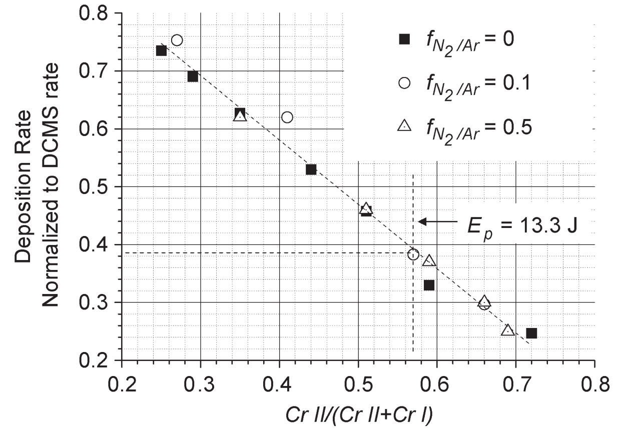

Fig. 3. HiPIMS deposition rate normalized to the DCMS rate (at the same average power) plotted as a function of the relative intensity of the optical emission line assigned to the Cr^+ ions. Data were acquired for different values of N_2-to-Ar flow ratio $f_{N_2/Ar}$ and for E_p between 3 and 30 J.

and 96.5% of the value typical for DCMS under the same conditions. In order to calculate the time-averaged effect of higher HiPIMS voltage, we need to take care of the fact that the amplitude of the target current (and thus, the ion flux incident on the target) varies largely throughout the pulse. Thus, we use instead the time-averaged sputtering efficiency $\overline{\gamma}$ where the sputtering-efficiency function $\gamma(t)$ is weighted with the target current over the time period of the pulse T

$$\bar{\gamma} = \frac{\int_0^T \gamma(t) I_{\rm HiPIMS}(t)dt}{\int_0^T I_{\rm HiPIMS}(t)dt}. \tag{8}$$

In this case, (8) yields $\overline{\gamma} = 88.25\%$. Although such drop in deposition rate should be certainly noticeable in the experiment, obviously, it does not explain the fact that the measured HiPIMS rate in metallic mode is only 40% of the corresponding DCMS rate. We therefore conclude that the influence of this effect on the deposition rate is a minor one, and other effects must dominate.

It is well known for HiPIMS discharges that the probability for ionization of sputter-ejected target species increases with increasing peak target current [8], [9]. As a consequence, the fraction of the sputtered material flux that gets captured by the cathode potential (causing resputtering) should also increase (assuming that the ion-capturing efficiency does not vary significantly with the peak target current). Thus, for any magnetron-sputtering system with ion-capturing efficiency that is larger than zero, the deposition rate is expected to drop with increasing peak target current. In order to quantify this effect for our system, the optical emission from Cr^+ ions (Cr II at 336.9 nm) and Cr neutrals (Cr I at 399.2 nm) was measured during HiPIMS discharge as a function of E_p (equivalent to the peak target current as the pulsewidth was fixed) for different N_2-to-Ar flow ratios $f_{N_2/Ar}$. The results were then used to plot the HiPIMS rate normalized to the DCMS rate as a function of the relative intensity of Cr II emission line (Cr $II/($Cr $II +$ Cr I)) shown in Fig. 3. The latter quantity represents *relative* changes of the metal-ion content in the plasma in the region close to the racetrack (cf. *Experimental Setup*). As evident from the figure, there is a linear drop of the DCMS-normalized

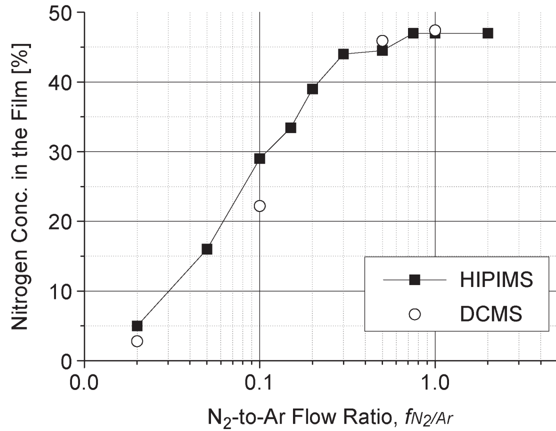

Fig. 4. Percentage of nitrogen in the sputter-deposited films as a function of the N_2-to-Ar flow ratio $f_{N_2/Ar}$. The same average power of 4 kW and substrate bias of 150 V were used for both HiPIMS and DCMS films.

HiPIMS rate with increasing signal strength of the Cr ions, independent of $f_{N_2/Ar}$. Moreover, the data points in Fig. 3 can be well fitted with a function of the form

$$y = 1.02 - 1.11x \tag{9}$$

where y is the HiPIMS-to-DCMS rate ratio and x stands for the relative ion content in the plasma. This particular form of the relationship between x and y indicates that the operational regime is close to that described by the target-pathway model of Christie [10] for the particular case where 1) the self-sputtering rate is similar to the Ar sputtering rate (which is well satisfied for Cr) and 2) almost all metal ions return back to the cathode (capturing efficiency close to unity). The $E_p = 13.3$ J that was used for deposition of all CrN_x films corresponds to the metal-ion content in the plasma of ~56% (cf. Fig. 3). For this ionization level, (9) yields the HiPIMS-to-DCMS deposition rate ratio of 0.38, which agrees very well with the data shown in Fig. 1 that indicate values between 0.33 and 0.4 ($f_{N_2/Ar}$ dependence). This result strongly suggests that the low HiPIMS rates measured in our setup are predominantly the effect of high ionization of sputtered material in combination with very effective Cr ion capture at the target. The high flux of metal ions usually observed further away from the target where the substrates to be coated are placed [39] may be due to back-reflected metal ions that got neutralized first at the target surface and still preserving significant portion of their kinetic energy gained in the cathode fall region and then become reionized on the way to the substrate. Alternatively, high plasma potentials that may temporarily reach tenths of volts during the high-power pulse (as indicated by the self-bias voltages reaching 100 V [18], [21], [39]) may also account for acceleration of ions generated further away from the cathode.

In Fig. 4 the atomic concentration of nitrogen in films prepared by HiPIMS and DCMS sputtering is shown as a function of $f_{N_2/Ar}$. Surprisingly, the films prepared by HiPIMS contain similar amounts of atomic nitrogen as the dc-sputtered samples grown at the corresponding value of the flow ratio $f_{N_2/Ar}$. Given the highly activated HiPIMS plasma present during the active phase of the discharge as well as the fact that the growing film is exposed to reactive gas for relatively long periods of time between the high-power pulses (3.1 ms, in this case), a nitrogen concentration was expected to greatly exceed that of dc-sputtered films. As this is apparently not the case, one can infer from these data that in the case of HiPIMS-deposited CrN_x, the rate of nitride formation at the substrate during the time between the high-power pulses must be negligibly low, as this would have otherwise lead to much higher nitrogen content in the HiPIMS films (with respect to corresponding films prepared by DCMS) at a given value of $f_{N_2/Ar}$. A somewhat higher nitrogen content observed in HiPIMS films grown at $f_{N_2/Ar} = 0.02$ and $f_{N_2/Ar} = 0.1$ does not contradict this conclusion, as we shall see hereafter. The upper limit for the amount of Cr delivered in each pulse to the substrate can be deduced from the data shown in Fig. 1. Even if the material flux from the target was composed of only sputter-ejected Cr species (which is not the case as it was shown that numerous N^+ and N_2^+ ions are detected even at lowest $f_{N_2/Ar}$ [39]), the amount of freshly deposited metal film per pulse would be on the order of 1/100 of a monolayer (ML) for $f_{N_2/Ar} = 0.02$ and dropping with increasing $f_{N_2/Ar}$ increases. On the other hand, the time necessary to convert one ML of deposited Cr into nitride (ML formation time, τ_{ML}) can be estimated using basic equations of kinetic gas theory [41]. The CrN ML formation time is then given by

$$\tau_{\mathrm{ML}} = \frac{1}{\eta z d_0^2} \tag{10}$$

where η is the sticking coefficient, d_0^2 stands for the area occupied on the surface by each adsorbed nitrogen atom, and z is the N_2 impingement rate. The latter can be calculated from

$$z = \frac{2p_{N_2}}{\sqrt{2\pi k T m_{N_2}}} \tag{11}$$

where p_{N_2} denotes partial pressure of N_2 gas, k is the Boltzmann constant, T is the gas temperature in kelvin, and m_{N_2} stands for the mass of N_2 molecule. The factor of two in the numerator of (11) accounts for the fact that each N_2 molecule supplies two nitrogen atoms. Assuming N_2 gas in the thermal equilibrium with the vacuum vessel and the surface density of N atoms of 2.3×10^{15} cm^{-2} (as in the CrN(100) crystal plane), by inserting (11) into (10), we can express the ML formation time as

$$\tau_{\mathrm{ML}}[s] = 1.27 \frac{f_{N_2/Ar} + 0.84}{\eta f_{N_2/Ar}} \times 10^{-3} \tag{12}$$

where we have also used the relation between the nitrogen partial pressure p_{N_2}, the total pressure during deposition p_{tot} (0.4 Pa), and the gas flow ratio $f_{N_2/Ar}$[3]

$$p_{N_2} = p_{\mathrm{tot}} \frac{f_{N_2/Ar}}{f_{N_2/Ar} + 0.84}. \tag{13}$$

[3]Here, we take into account nonequal pumping speeds for N_2 and Ar that were determined experimentally for our system. We also assume that the partial pressure of N_2 in the vicinity of the substrate is not affected by the gas rarefaction effects. This assumption is well justified by the fact that the sample-to-target distance is 7 cm, i.e., large on the scale of usually observed changes in gas density. Moreover, these effects are predominantly present during the high-power pulses, whereas here, we are considering N_2 adsorption in the pulse-off phase.

Using (12), the critical N_2-to-Ar flow rate required for the amount of Cr deposited in each pulse to react during the time period between the pulses, τ_{OFF}, can be deduced by imposing the condition

$$\tau_{OFF} = 10^{-2}\tau_{ML} \tag{14}$$

where we have used the upper estimate for the amount of Cr deposited in each pulse (1/100 of an ML). By inserting (12) into (14) and setting $\tau_{OFF} = 3.1$ ms (300 Hz and 200 μs pulsewidth), we arrive at

$$f_{N_2/Ar}(\tau_{OFF} = 10^{-2}\tau_{ML}) = \frac{0.84}{244.09\eta - 1}. \tag{15}$$

Thus, if the ambient N_2 should efficiently react with the freshly deposited Cr film during the time between the pulses (implying $\eta = 1$), the nitrogen content in the film would have reached a saturation level of 45–47 at% already at $f_{N_2/Ar} \approx 0.003$. As shown in Fig. 4, the nitrogen content increases gradually to saturate not earlier than at $f_{N_2/Ar} \approx 0.3$, thus at 100 times higher flow ratio. The upper limit for the sticking coefficient can be obtained from (15) by imposing that all nitrogen found in the films prepared at $f_{N_2/Ar} = 0.3$ was adsorbed between the high-power pulses. This yields $\eta \leq 0.016$ and, most likely, even this small number is largely overestimating the N_2 uptake rate in the pulse-off phase as significant incorporation of nitrogen is expected to take place during the high-power pulse due to high concentration of energetic N^+ and N_2^+ species detected in the plasma [39].

Our observations are in a good agreement with the experimental evidence from the literature. It has been shown [42] that the freshly deposited chromium film does not react with N_2 to form CrN_x at $T < 500$ K. Additional factors are necessary to trigger the reaction, like, e.g., a high density of chemically activated nitrogen species that is likely present during the active phase of the HiPIMS discharge. In view of this, it is therefore suggested that nitrogen incorporation into the growing CrN_x film proceeds predominantly during the high-power pulses.

The results shown in Fig. 4 contradict to some extent what has already been reported for HiPIMS processing. For instance, Böhlmark *et al.* [43] showed that lower flows of reactive gas are required to form stoichiometric TiN by HiPIMS than by conventional DCMS. This discrepancy can be rationalized by the fact that the enthalpy of CrN formation is relatively low as compared with TiN (−117.15 versus −337.65 kJ/mol, respectively) that may very well account for low N uptake rate between the pulses. In order to verify this point, we have also sputtered Ti target under similar conditions ($T_S = 200\,°\mathrm{C}$, $P = 4$ kW, $f = 300$ Hz, and $V_S = 150$ V). The stoichiometric TiN was obtained already at the lowest N_2-to-Ar flow ratio tested, $f_{N_2/Ar} = 0.02$, i.e., at the process point where the corresponding CrN_x film contained only 5 at% of N. This comparison suggests that reactivity towards nitrogen may steer the film-growth process during HiPIMS to much larger extent than it is the case during DCMS. For metals that exhibit higher reactivity toward working gas mixture, the compound formation could proceed also during the pulse-off phase (predominantly by absorption of molecular N_2), whereas in the case of less-reactive metals, the chemistry would be limited to the active phase of the discharge where highly activated species are present (N_2^+, N^+, etc.).

To complete the discussion of sample composition, it may be added that the oxygen content in films prepared by HiPIMS was on the same (low) level as in films prepared by DCMS, usually not exceeding 0.1 at%. No Ar impurities were found in HiPIMS samples (below the 0.1 at% detection limit of ToF-ERDA), while films prepared by DCMS showed Ar content between 0.1 and 0.3 at%. This difference may be explained by severe gas rarefaction effects observed during HiPIMS processing that make the total Ar^+ ion-count rate go down in the middle of the high-power pulse [39].

The apparent understoichiometry of the CrN films prepared at higher values of $f_{N_2/Ar}$ is a consequence of the high bias voltage used (150 V). It is interesting to note that the preferential resputtering of nitrogen (manifested by a decrease in both the nitrogen content and the total film thickness with increasing bias voltage) is not more severe in the case of samples prepared by HiPIMS. This is despite the significantly higher flux of energetic Cr^+ and Cr^{2+} ions (with respect to the conventional dc sputtering) present during HiPIMS deposition, as will be shown next. It is a promising result, particularly since high fluxes of film-forming ions are, in many cases, beneficial for film growth.

Fig. 5 shows a set of cross-sectional SEM micrographs revealing the film microstructure as a function of $f_{N_2/Ar}$ for HiPIMS [Fig. 5(a) to (d)] and DCMS [Fig. 5(e) to (h)] samples. The corresponding $\theta-2\theta$ XRD scans are shown in Fig. 6(a) (HiPIMS) and Fig. 6(b) (DCMS). The purely metallic films [Fig. 6(a) vs (e)] exhibit columnar structure with a typical signature of a competitive growth that results in the column width increasing with increasing film thickness. The film grown by DCMS process possesses strong $\langle 200\rangle$ texture, while the HiPIMS film is $\langle 210\rangle$-textured. Addition of a small amount of nitrogen to the gas mixture leads to radical changes in the microstructure of the HiPIMS-deposited coatings. Already, at $f_{N_2/Ar} = 0.02$ [cf. Fig. 5(b)], corresponding to 5 at% nitrogen in the film, the columnar growth is completely suppressed, and the film is composed of nanosized grains. The film is characterized by an extremely low surface roughness that hardly gives any contrast in the SEM (the average surface roughness R_a deduced from the atomic force microscopy investigations is 0.25 nm [44]). This effect is also observed for films grown at $f_{N_2/Ar} = 0.1$ (Fig. 5(c), with a nitrogen content of 29 at%) and for a few more samples (not shown here) up to the nitrogen content of ~33 at% (corresponding to $f_{N_2/Ar} \approx 0.15$). A more detailed examination of XRD data reveals that this effect is restricted to those films that are composed of a solid solution Cr(N) and hexagonal β-Cr_2N phases and do not contain cubic CrN phase.

The phase identification was performed by means of the tilt-angle-dependent XRD analysis [44]. In order to facilitate comparison between the two sputtering methods, the XRD data shown in Fig. 6 are presented for the case where the diffraction plane was perpendicular to the target surface. It can be seen that the loss of a columnar growth for the samples shown in Fig. 5(b) and (c) is reflected in the corresponding diffractograms [cf. Fig. 6(a)]: the Cr(110) peak becomes

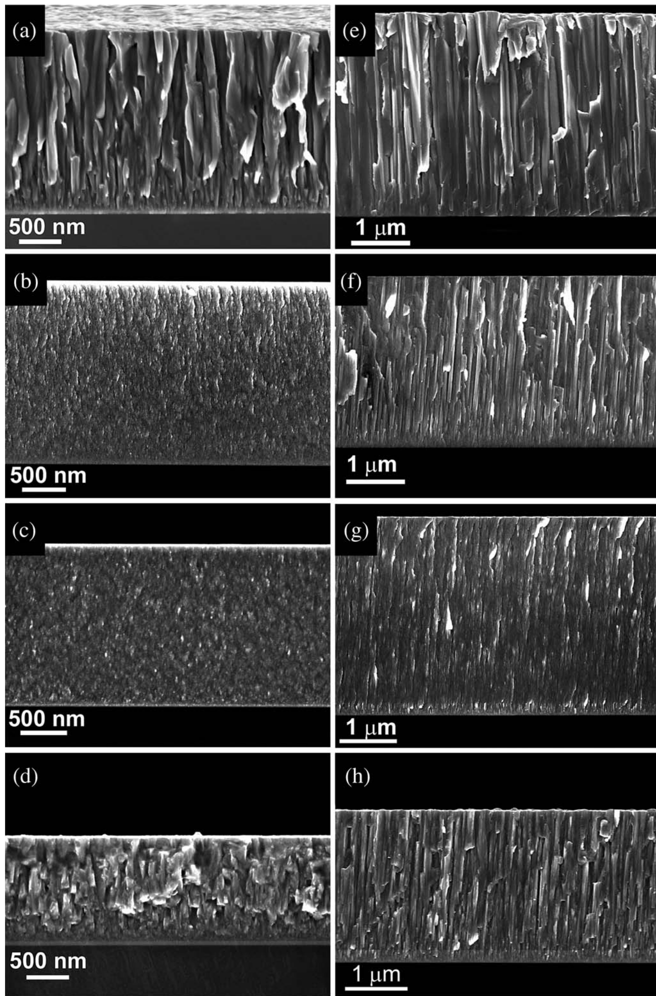

Fig. 5. Fracture cross-sectional SEM micrographs illustrating the effect of microstructure evolution upon increasing $f_{N_2/Ar}$ for both (left column, graphs a–d) HiPIMS- and (right column, graphs e–h) DCMS films. The flow ratios and the nitrogen content in the film are as follows: a) $f_{N_2/Ar} = 0$, 0 at%; b) $f_{N_2/Ar} = 0.02$, 5 at%; c) $f_{N_2/Ar} = 0.1$, 29 at%; d) $f_{N_2/Ar} = 0.5$, 44 at%; e) $f_{N_2/Ar} = 0$, 0 at%; f) $f_{N_2/Ar} = 0.02$, 3 at%; g) $f_{N_2/Ar} = 0.1$, 22 at%; and h) $f_{N_2/Ar} = 0.5$, 46 at%. Note that different scales are used for HiPIMS and DCMS films.

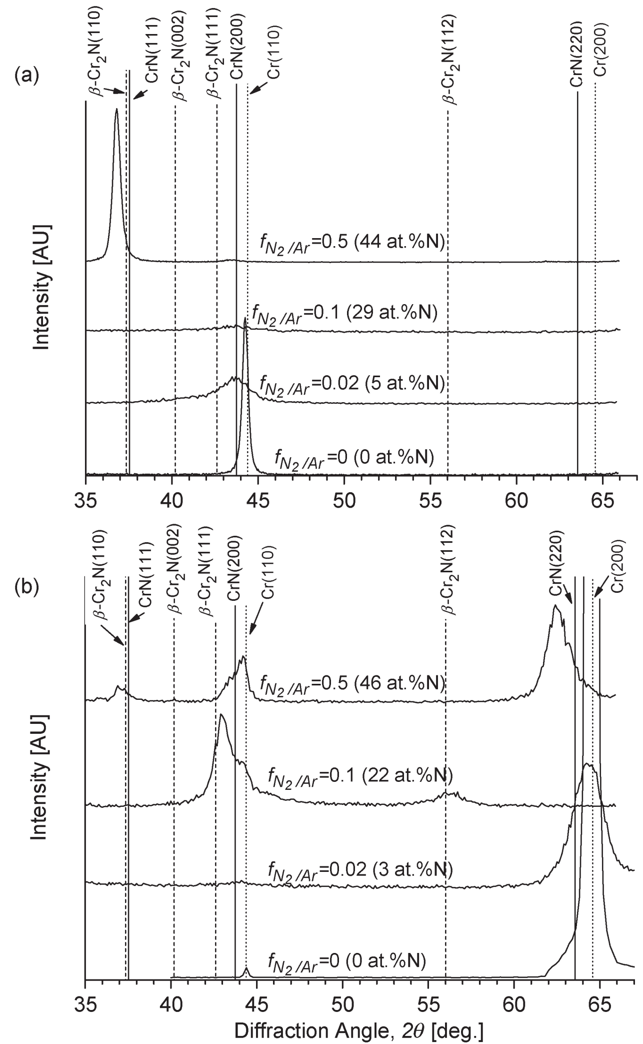

Fig. 6. $\theta-2\theta$ XRD scans performed on (a) HiPIMS and (b) DCMS films as a function of the nitrogen content in the films.

extremely broad at $f_{N_2/Ar} = 0.02$, and eventually, the XRD spectra becomes featureless at $f_{N_2/Ar} = 0.1$, confirming the nanocrystalline growth mode. At higher nitrogen flows, the signature of a columnar growth is again present as evident from the SEM micrographs [Fig. 5(d)] as well as from the XRD data in Fig. 6(a) $(f_{N_2/Ar} = 0.5)$ that also indicate the $\langle 111 \rangle$-textured films. The CrN(111) peak in the latter case is shifted toward a lower diffraction angle as a result of residual compressive stress. It is thus evident that the column-free growth phenomenon observed here is of a different nature than it was with the case for the HiPIMS-grown nanocrystaline CrN film previously reported by Alami *et al.* [19]. First of all, it occurs exclusively for low-N-content films dominated by Cr(N) and β-Cr_2N phases, whereas others reported that it occurs on films dominated by CrN phase that are clearly columnar in our case. Second, the authors in [19] did not observe any change in surface roughness as the film morphology evolved from columnar to featureless upon increase of the amplitude of the peak target current. This remains in contrast to our findings [44] where columnar films were characterized by average surface roughness which is an order of magnitude higher. Moreover, it is not clear whether the effect reported in [19] was exclusively due to the increase of peak target current as the pulsing frequency was varied simultaneously. Perhaps a similar phenomenon was reported for stoichiometric CrN films prepared by MPP sputtering technique. Lin *et al.* [29] obtained fine-grain films at high nitrogen flow (N_2-to-Ar gas flow ratio of one). Note that in the latter case, surface roughness between 5.7 and 8.2 nm was reported, which is more than an order of magnitude higher than that measured on our films [44]. Another important fact is that, in the present case, a high substrate bias voltage was necessary to disturb the columnar growth and produce nanocrystaline films. We have shown [44] that the grain size increases with lowering bias and, as a consequence, even low-nitrogen-content films are columnar if deposited at substrate bias of 60 V or lower. We note that the nanocrystaline CrN films reported previously were prepared either at self-bias [29] or for grounded substrates [19], again pointing toward a different nature of reported phenomenon.

The structure-free SEM cross sections have been also observed previously for CrN$_x$ films deposited using closed-field unbalanced magnetron-sputtering technique by Hurkmans *et al.* [45] for a similar substrate temperature (250 °C) and high substrate bias (100 V) as in our case. The phenomenon was, however, limited only to samples containing the hexagonal closed-packed β-Cr_2N phase, with 20.5–33 at% nitrogen, whereas samples with lower (7.5 at%) and higher (46.5 at%) nitrogen content were characterized by a dense columnar structure. Such results were also reported by Rebholz *et al.* [46] (featureless SEM cross sections at a nitrogen content of 29 at%).

In the present case, the evolution of a microstructure of dc-sputtered films with increasing $f_{N_2/Ar}$ is clearly different and stays in contrast to the results obtained in HiPIMS processing. As evident from the set of cross-sectional SEM micrographs shown in Fig. 5(e)–(h), the columnar-growth mode is preserved over the entire range of flow ratios examined. This is valid in particular for the low-nitrogen content samples shown in Fig. 5(f) and (g), which contain 3 at% N and 22 at% N, respectively. The broadening of the corresponding XRD peaks [cf. Fig. 6(b)] indicates that the crystallite size decreases upon incorporation of nitrogen, although not to the extent observed for HiPIMS samples [cf. data scans for $f_{N_2/Ar} = 0.02$ and $f_{N_2/Ar} = 0.1$ in Fig. 6(a) and (b)]. In-depth analysis reveals that in the case of the sample prepared at $f_{N_2/Ar} = 0.02$ [cf. Fig. 5(f)], nitrogen dissolves in the original bcc-Cr lattice forming interstitial compound. The film shown in Fig. 5(g)($f_{N_2/Ar} = 0.1$) is dominated by the β-Cr_2N phase, while the CrN-phase constituted a sample grown at $f_{N_2/Ar} = 0.5$ [Fig. 5(h)]. The latter sample exhibits the $\langle 220 \rangle$ texture, which is in contrast to the film prepared under the same $f_{N_2/Ar}$ with HiPIMS. This difference is likely the result of highly energetic ion bombardment during HiPIMS processing.

Fig. 7 shows the relative composition of the ion flux incident upon the growing film during HiPIMS (a) and DCMS (b) discharge, as a function of the N_2-to-Ar ratio $f_{N_2/Ar}$. Note that in the former case, the time-averaged data (thus including also the contribution due to the ion flux present between the pulses) are shown. The commonly reported metallic character of the HiPIMS plasma [11], [21], [47] is evident: The Cr^+ ions constitute the strongest contribution up to $f_{N_2/Ar} = 2$ (where the N_2^+ signal takes over), which is quite the opposite to the DCMS case where the working-gas ions dominate the ion flux to the substrate (Ar^+ ions up to $f_{N_2/Ar} = 0.8$ and N_2^+ ions at higher nitrogen content). In addition, the relative intensity of the Cr^{2+} signal is strongly increased during the HiPIMS operation, and the relative contribution due to these species varies between 2% and 3%, while the highest value recorded in the DCMS mode is only 0.13% ($f_{N_2/Ar} = 0$) and decreases with increasing $f_{N_2/Ar}$ down to 0.05%. This highly increased number of Cr^{2+} ions is believed to account for the suppression of the columnar growth (at lower $f_{N_2/Ar}$) in the case of HiPIMS deposition. This was concluded from the fact that the occurrence of the column-free growth is a function of the substrate bias (occurs for bias voltages higher than 100 V [44]) and, as such, cannot only be ascribed to the specific nature of the pulsed deposition. It is evident that a combination of a high substrate bias and a high flux of doubly charged Cr ions are sufficient conditions for the disruption of the grain growth and renucleation. Since only a small fraction of an ML gets deposited in a single pulse, this process is highly effective in reducing the average grain size to the nanometer level.

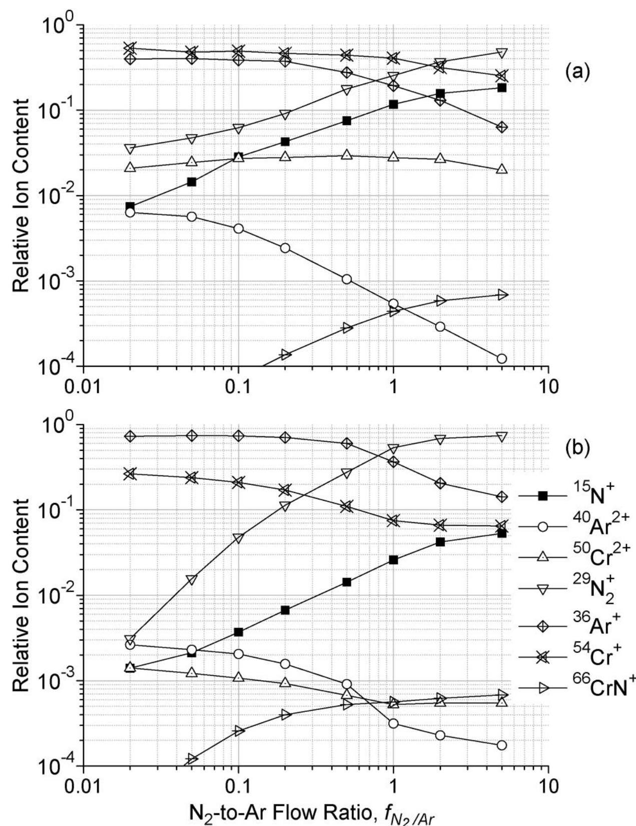

Fig. 7. Relative ion content in the flux incident upon the substrate during (a) HiPIMS and (b) DCMS process, plotted versus the N_2-to-Ar flow ratio $f_{N_2/Ar}$.

Another major difference between HiPIMS and DCMS is related to the ions of a reactive gas incident upon the growing film. In the latter case, majority of nitrogen ions arrive in the form of N_2^+ (typically an order of magnitude higher intensity than for the atomic nitrogen ions), while the N^+ ions constitute a significantly higher contribution during HiPIMS operation, accounting for roughly half the intensity of the N_2^+ ion flux. The difference becomes even more pronounced if one considers the ion-flux composition during the high-power pulse only, thus neglecting the ions arriving in the postdischarge HiPIMS plasma. The time- and energy-resolved data reported separately [39] indicate that the N^+ ions constitute the primary source of nitrogen ions detected during the HiPIMS pulse and, for $f_{N_2/Ar} \geq 0.3$, are the second highest contribution to the total energy flux. In addition, the N^+ ions are by far more energetic than the N_2^+ ions, with the high-energy tail similar to that observed for the target metal ions (Cr^+ and Cr^{2+}). The reason for a higher N^+ content in the case of a HiPIMS plasma was attributed to a very high temporal energy density on the target that could enhance the dissociative sputtering of CrN as well as lead to a more effective decomposition of the back-reflected N_2^+ ions. In fact, the data shown in Fig. 7 support the dissociative sputtering of CrN in the case of a HiPIMS process: The relative

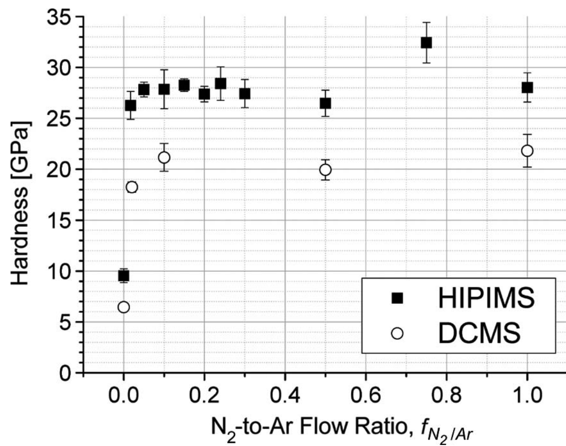

Fig. 8. Nanoindentation hardness data as a function of the N_2-to-Ar flow ratio $f_{N_2/Ar}$ for both sputtering techniques.

contribution from the CrN^+ ions is lower than from DCMS, at least, for lower $f_{N_2/Ar}$ values.

The mechanical properties of the films deposited by the two sputtering techniques are compared in Fig. 8, where the nanoindentation hardness is plotted as a function of the N_2-to-Ar flow ratio $f_{N_2/Ar}$. It can be seen that HiPIMS yields better properties already in the case of metallic films ($f_{N_2/Ar} = 0$) where nearly 50% harder films are obtained (9.5 versus 6.4 GPa for HiPIMS and DCMS, respectively). However, for both sputtering techniques, an incorporation of a small amount of nitrogen leads to a dramatic increase in the film hardness. This effect can be ascribed to the following: 1) the solid solution strengthening caused by the nitrogen atoms that induce point defects in the original Cr crystal lattice and in this way impede dislocation motion and 2) the grain-size hardening from the apparent reduction of the average crystallite size that impede glide of dislocations between grains of different orientation. The fact that the latter effect is more pronounced in the case of HiPIMS (as evident from the XRD peak broadening, cf. Fig. 6) may explain higher hardness values that, for the column-free films, oscillate between 26.3 GPa ($f_{N_2/Ar} = 0.02$) and 27.9 GPa ($f_{N_2/Ar} = 0.1$). This is a significant increase as compared with the hardness of the DCMS films that show a stepwise increase, first to 18.2 GPa at $f_{N_2/Ar} = 0.02$ and then up to 21.1 GPa at $f_{N_2/Ar} = 0.1$. No clear trend is observed at higher $f_{N_2/Ar}$ values for any of the sputtering techniques. In particular, the transition from the column-free growth to the columnar-growth mode (taking place for HiPIMS samples at $f_{N_2/Ar} \geq 0.15$) accompanied by the gradual transformation from films dominated by the hexagonal β-C_2N phase to films dominated by the CrN phase does not have any obvious influence on the film hardness. High residual-stress levels found in films grown at $f_{N_2/Ar} \geq 0.3$ and ranging from -7.1 GPa at $f_{N_2/Ar} = 0.3$ to -9.6 GPa at $f_{N_2/Ar} = 1$ may also affect hardness within this regime. The low N-content films ($f_{N_2/Ar} < 0.3$) exhibit moderate stress between -1.5 and -3.8 GPa, which should not have a dominant effect on film hardness.

These, at first surprising, results may be in fact be interpreted with the help of a previously reported data. First of all, in the work of Hurkmans *et al.* [45], the hardness was shown to increase monotonically with increasing nitrogen content in the film to reach the maximum for the sample containing 20.5 at% of nitrogen. For the nitrogen content in the range between 20.5 and 33 at%, a decrease in film hardness was observed (to the level typical for films containing only 7.5 at% nitrogen) and only a slight increase for films with higher nitrogen content (measured up to 46.5 at%). The film with maximum hardness contained understoichiometric β-C_2N phase and was characterized by a featureless appearance in cross-sectional SEM. Similar evolution of hardness with increasing nitrogen content in the dc-sputtered CrN_x film was also reported by Mayrhofer *et al.* [48]. In their case, however, the maximum hardness was obtained for the film containing 33 at% of nitrogen (corresponding to the stoichiometric β-C_2N phase) that was deposited at $f_{N_2/Ar} = 0.25$. More importantly, it was shown that this type of dependence is typical for films grown under low-energy ion bombardment (ion energy of less than 32 eV) conditions, whereas exposure to the flux of the high-energy ions (energies between 87 and 101 eV) resulted in films with no clear correlation between the hardness and the crystallinity (after an initial increase, when going from 0 to 13 at% nitrogen, the hardness did not change significantly with increasing $f_{N_2/Ar}$ [48]). In view of these results, it is thus not surprising that films prepared by HiPIMS, where a high flux of highly energetic ions is inherently present, show no direct relationship between the film hardness and the nitrogen content, for $f_{N_2/Ar} > 0$. For the hardness of our dc-sputtered films, the obtained values at $f_{N_2/Ar} = 0.1$ and $f_{N_2/Ar} = 0.5$ correspond very well to the side points on both sides of the hardness maximum reported by Mayrhofer *et al.* [48].

IV. Conclusions

CrN_x films with varying nitrogen content synthesized in the same vacuum system using reactive HiPIMS and conventional DCMS have been analyzed and compared. Depending on the N_2-to-Ar flow ratio $f_{N_2/Ar}$, the deposition rate of HiPIMS varied between 40% ($f_{N_2/Ar} = 0$) and 33% ($f_{N_2/Ar} = 1$) of that of the DCMS case, both at the same average power. The HiPIMS deposition rate relative to the DCMS rate was found to decrease linearly with increasing relative signal strength from the Cr ions. This allowed for the interpretation of rate drop in terms of the target-pathway model in which low deposition rates are a direct consequence of the high ionization level ($\sim$56% here) of the target material and effective Cr ion capture by the cathode potential. The effect of higher target voltage on lowering of the HiPIMS deposition rate was shown to be of a minor importance in this case.

Both sputtering techniques showed a similar drop in the deposition rate with increasing $f_{N_2/Ar}$ when referred to the metallic mode of operation. Also, the nitrogen content in the films grown at a given flow ratio $f_{N_2/Ar}$ was very similar in both cases.

It was concluded that the HiPIMS film stoichiometry is determined by the plasma composition during active phase of the discharge, and the nitrogen uptake at the substrate during the time between the pulses is negligible.

The microstructure evolution of HiPIMS-sputtered films with increasing $f_{N_2/Ar}$ clearly differs from that in dc-sputtered

samples. For HiPIMS films containing less than ∼33 at% nitrogen, the fracture cross-sectional SEM micrographs reveal a columnless growth mode with nanosized grains, while the DCMS films exhibit columnar growth independent of $f_{N_2/Ar}$. The combination of a high substrate bias and a high flux of doubly charged Cr ions present in the HiPIMS discharge results in the disruption of the grain growth and renucleation.

HiPIMS films also have a higher hardness over the entire range of gas compositions. The lack of any particular dependence of the hardness on the crystalline content in the case of HiPIMS samples is considered to be typical for samples prepared using high-energy ion flux.

REFERENCES

[1] C. Christou and Z. H. Barber, "Ionization of sputtered material in a planar magnetron discharge," *J. Vac. Sci. Technol. A, Vac. Surf. Films*, vol. 18, p. 6, 2000.

[2] P. J. Kelly and R. D. Arnell, "Magnetron sputtering: A review of recent developments and applications," *Vacuum*, vol. 56, no. 3, pp. 159–172, Mar. 2000.

[3] P. Sigmund, "Sputtering of single and multiple component materials," *J. Vac. Sci. Technol. A, Vac. Surf. Films*, vol. 17, no. 1, p. 396, Jan. 1979.

[4] M. W. Thompson, "Physical mechanisms of sputtering," *Phys. Rep.*, vol. 69, no. 4, pp. 335–371, Mar. 1981.

[5] J. A. Hopwood, Ed., "Ionized physical vapor deposition," in *Thin Films*. San Diego, CA: Academic, 2000.

[6] V. Kouznetsov, K. Macak, J. M. Schneider, U. Helmersson, and I. Petrov, "A novel pulsed magnetron sputter technique utilizing very high target power densities," *Surf. Coat. Technol.*, vol. 122, no. 2/3, p. 290, Dec. 1999.

[7] J. Bohlmark, J. T. Gudmundsson, J. Alami, M. Lattemann, and U. Helmersson, "Spatial electron density distribution in a high-power pulsed magnetron discharge," *IEEE Trans. Plasma Sci.*, vol. 33, no. 2, p. 346, Apr. 2005.

[8] U. Helmersson, M. Lattemann, J. Bohlmark, A. P. Ehiasarian, and J. T. Gudmundsson, "Ionized physical vapor deposition (IPVD): A review of technology and applications," *Thin Solid Films*, vol. 513, no. 1/2, pp. 1–24, Aug. 2006.

[9] K. Sarakinos, J. Alami, and S. Konstantinidis, "High power pulsed magnetron sputtering: A review on scientific and engineering state of the art," *Surf. Coat. Technol.*, vol. 204, no. 11, pp. 1661–1684, Feb. 2010.

[10] D. J. Christie, "Target material pathways model for high power pulsed magnetron sputtering," *J. Vac. Sci. Technol. A, Vac. Surf. Films*, vol. 23, no. 2, p. 330, Mar. 2005.

[11] J. Vlcek, P. Kudlacek, K. Burcalova, and J. Musil, "High-power pulsed sputtering using a magnetron with enhanced plasma confinement," *J. Vac. Sci. Technol. A, Vac. Surf. Films*, vol. 25, no. 1, pp. 42–47, Jan. 2007.

[12] A. Anders, "Deposition rates of High Power Impulse Magnetron Sputtering," in *Proc. 51th Annu. SVC Tech. Conf.*, Chicago, IL, Apr. 19–24, 2008, p. 271.

[13] K. Sarakinos, J. Alami, J. Dukwen, J. Woerdenweber, and M. Wuttig, "Refinement of Monte Carlo simulations of electron–specimen interaction in low-voltage SEM," *J. Phys. D, Appl. Phys.*, vol. 41, no. 21, p. 215 310, Oct. 2008.

[14] D. Lundin, P. Larsson, E. Wallin, M. Lattemann, N. Brenning, and U. Helmersson, "Cross-field ion transport during high power impulse magnetron sputtering," *Plasma Sources Sci. Technol.*, vol. 17, no. 3, p. 035 021, Jul. 2008.

[15] J. Emmerlich, S. Mráz, R. Snyders, K. Jiang, and J. M. Schneider, "The physical reason for the apparently low deposition rate during high-power pulsed magnetron sputtering," *Vacuum*, vol. 82, no. 8, pp. 867–870, Apr. 2008.

[16] R. Chistyakov, B. Abraham, W. Sproul, J. Moore, and J. Lin, "Modulated pulse power technology and deposition for protective and tribological coatings," in *Proc. 50th Annu. SVC Tech. Conf.*, Louisville, KY, Apr. 30–May 3, 2007, pp. 139–143.

[17] R. Chistyakov, B. Abraham, and W. D. Sproul, "Advances in high power pulsed reactive magnetron sputtering," in *Proc. 49th Annu. SVC Tech. Conf.*, Washington, DC, Apr. 23–27, 2006, pp. 16–19.

[18] A. P. Ehiasarian, P. E. Hovsepian, L. Hultman, and U. Helmersson, "Comparison of microstructure and mechanical properties of chromium nitride-based coatings deposited by high power impulse magnetron sputtering and by the combined steered cathodic arc/unbalanced magnetron technique," *Thin Solid Films*, vol. 457, no. 2, pp. 270–277, Jun. 2004.

[19] J. Alami, K. Sarakinos, F. Uslu, and M. Wuttig, "On the relationship between the peak target current and the morphology of chromium nitride thin films deposited by reactive high power pulsed magnetron sputtering," *J. Phys. D, Appl. Phys.*, vol. 42, no. 1, p. 015 304, Jan. 2009.

[20] K. Bobzin, N. Bagcivan, P. Immich, S. Bolz, R. Cremer, and T. Leyendecker, "Mechanical properties and oxidation behaviour of (Al,Cr)N and (Al,Cr,Si)N coatings for cutting tools deposited by HPPMS," *Thin Solid Films*, vol. 517, no. 3, pp. 1251–1256, Dec. 2008.

[21] A. P. Ehiasarian, W.-D. Munz, L. Hultman, U. Helmersson, and I. Petrov, "High power pulsed magnetron sputtered CrN_x films," *Surf. Coat. Technol.*, vol. 163/164, pp. 267–272, Jan. 2003.

[22] P. E. Hovsepian, C. Reinhard, and A. P. Ehiasarian, "CrAlYN/CrN superlattice coatings deposited by the combined high power impulse magnetron sputtering/unbalanced magnetron sputtering technique," *Surf. Coat. Technol.*, vol. 201, no. 7, pp. 4105–4110, Dec. 2006.

[23] S. Konstantinidis, J. P. Dauchot, and M. Hecq, "Titanium oxide thin films deposited by high-power impulse magnetron sputtering," *Thin Solid Films*, vol. 515, no. 3, pp. 1182–1186, Nov. 2006.

[24] S. Konstantinidis, A. Hemberg, J. P. Dauchot, and M. Hecq, "Deposition of zinc oxide layers by high-power impulse magnetron sputtering," *J. Vac. Sci. Technol. B, Microelectron. Process. Phenom.*, vol. 25, no. 3, pp. L19–L21, 2007.

[25] J. Paulitsch, P. H. Mayrhofer, W.-D. Münz, and M. Schenkel, "Structure and mechanical properties of CrN/TiN multilayer coatings prepared by a combined HiPIMS/UBMS deposition technique," *Thin Solid Films*, vol. 517, no. 3, pp. 1239–1244, Dec. 2008.

[26] G. Sáfrán, C. Reinhard, A. P. Ehiasarian, P. B. Barna, L. Székely, O. Geszti, and P. E. Hovsepian, "Influence of the bias voltage on the structure and mechanical performance of nanoscale multilayer CrAlYN/CrN physical vapor deposition coatings," *J. Vac. Sci. Technol. A, Vac. Surf. Films*, vol. 27, p. 174, 2009.

[27] V. Sittinger, F. Ruske, C. Gerloff, W. Werner, B. Szyszka, and D. J. Christie, "Deposition of high conductivity ITO films by High Power Pulsed Magnetron Sputtering (HPPMS)," in *Proc. 49th Annu. SVC Tech. Conf.*, Washington, DC, Apr. 23–27, 2006, p. 16.

[28] E. Wallin, T. I. Selinder, M. Elfwing, and U. Helmersson, "Synthesis of α-Al_2O_3 thin films using reactive high-power impulse magnetron sputtering," *Europhys. Lett.*, vol. 82, no. 3, p. 36 002, Apr. 2008.

[29] J. Lin, J. J. Moore, W. D. Sproul, B. Mishra, Z. Wu, and J. Wang, "The structure and properties of chromium nitride coatings deposited using dc, pulsed dc and modulated pulse power magnetron sputtering," *Surf. Coat. Technol.*, vol. 204, no. 14, pp. 2230–2239, Apr. 2010.

[30] W.-D. Munz, D. Schulze, and F. J. M. Hauzer, "A new method for hard coatings: ABS (arc bond sputtering)," *Surf. Coat. Technol.*, vol. 50, no. 2, pp. 169–178, Feb. 1992.

[31] [Online]. Available: http://www.cemecon.de/information/news/hppms__high_plasma_ionisation/index_eng.html

[32] M. S. Janson, "CONTES, Conversion of Time-Energy Spectra, a Program for ERDA Data Analysis," Uppsala Univ., Uppsala, Sweden, 2004.

[33] W. C. Oliver and G. M. Pharr, "An improved technique for determining hardness and elastic modulus using load and displacement sensing indentation experiments," *J. Mater. Res.*, vol. 7, no. 6, pp. 1564–1583, Jun. 1992.

[34] J. Bohlmark, M. Lattemann, J. T. Gudmundsson, A. P. Ehiasarian, Y. A. Gonzalvo, N. Brenning, and U. Helmersson, "The ion energy distributions and ion flux composition from a high power impulse magnetron sputtering discharge," *Thin Solid Films*, vol. 515, no. 4, pp. 1522–1526, Dec. 2006.

[35] Private communication with the manufacturer of the mass spectrometer, Hiden Analytical, U.K.

[36] J. A. Davis, W. D. Sproul, D. J. Christie, and M. Geisler, "High Power Pulse Reactive Sputtering of TiO_2," in *Proc. 47th Annu. SVC Tech. Conf.*, Dallas, TX, 2004, p. 215.

[37] D. A. Glocker, M. M. Romach, D. J. Christie, and W. D. Sproul, "High Power Pulsed Reactive Sputtering of Zirconium Oxide and Tantalum Oxide," in *Proc. 47th Annu. SVC Tech. Conf.*, Dallas, TX, 2004.

[38] W. D. Sproul, D. J. Christie, and D. C. Carter, "The Reactive Sputter Deposition of Aluminum Oxide Coatings Using High Power Pulsed Magnetron Sputtering (HPPMS)," in *Proc. 47th Annu. SVC Tech. Conf.*, Dallas, TX, 2004.

[39] G. Greczynski and L. Hultman, "Time and energy resolved ion mass spectroscopy studies of the ion flux during high power pulsed magnetron sputtering of Cr in Ar and Ar/N_2 atmospheres," *Vacuum*, vol. 84, no. 9, pp. 1159–1170, Apr. 2010.

[40] J. F. Ziegler and J. Biersack, Monte Carlo Code SRIM-2008.042010. [Online]. Available: www.srim.org

[41] J. F. O'Hanlon, *A User Guide to Vacuum Technology*. Hoboken, NJ: Wiley, 2003, pp. 9–15.

[42] W. Ensinger and M. Kiuchi, "The formation of chromium/nitrogen phases by nitrogen ion implantation during chromium deposition as a function of ion-to-atom arrival ratio," *Surf. Coat. Technol.*, vol. 94/95, pp. 433–436, Oct. 1997.

[43] J. Böhlmark, M. Lattemann, H. Stranning, T. Selinder, J. Carlsson, and U. Helmersson, "Reactive Film Growth of TiN by Using High Power Impulse Magnetron Sputtering (HiPIMS)," in *Proc. 49th Annu. Tech. Conf.*, Washington, DC, 2006.

[44] G. Greczynski, J. Jensen, J. Bohlmark, and L. Hultman, "Microstructure control of CrNx films during high power impulse magnetron sputtering," *Surf. Coat. Technol.*, vol. 205, pp. 118–130, 2010.

[45] T. Hurkmans, D. B. Lewis, J. S. Brooks, and W.-D. Munz, "Chromium nitride coatings grown by unbalanced magnetron (UBM) and combined arc/unbalanced magnetron (ABS) deposition techniques," *Surf. Coat. Technol.*, vol. 86/87, pp. 192–199, Dec. 1996.

[46] C. Rebholz, H. Ziegele, A. Leyland, and A. Matthews, "Structure, mechanical and tribological properties of nitrogen-containing chromium coatings prepared by reactive magnetron sputtering," *Surf. Coat. Technol.*, vol. 115, no. 2/3, pp. 222–229, Jul. 1999.

[47] J. Bohlmark, J. Alami, C. Christou, A. P. Ehiasarian, and U. Helmersson, "Ionization of sputtered metals in high power pulsed magnetron sputtering," *J. Vac. Sci. Technol. A, Vac. Surf. Films*, vol. 23, no. 1, pp. 18–22, Jan. 2005.

[48] P. H. Mayrhofer, G. Tischler, and C. Mitterer, "Microstructure and mechanical/thermal properties of Cr–N coatings deposited by reactive unbalanced magnetron sputtering," *Surf. Coat. Technol.*, vol. 142–144, pp. 78–84, Jul. 2001.

Grzegorz Greczynski received the M.Sc. degree in physics from the University of Science and Technology in Cracow, Krakow, Poland, and the Ph.D. degree in material science from Linköping University, Linköping, Sweden, in 2001 for the work on the photoelectron spectroscopy studies of metal-organic surfaces and interfaces.

Between 2001 and 2006 he was with ThinFilm Electronics AB (Sweden), working on the development of nonvolatile thin-film-based memories. During the period 2006–2008, he was the R&D Manager with the original HiPIMS company–Chemfilt Ionsputtering AB. He is currently a Senior Research Engineer with the Thin Film Physics Division, Department of Physics, Linköping University, headed by Prof. Lars Hultman. His main research interests include reactive sputter deposition of binary and ternary transition metal nitrides using HiPIMS.

Jens Jensen received the Ph.D. degree in physics from Syddansk Universitet, Odense, Denmark in 1999.

He is currently a University Lecturer with the Department of Physics, Chemistry, and Biology, Linköping University, Linköping, Sweden. His main research concerns different aspects on ion interaction with surfaces related to material modification and analysis, with particular interest in ion beam synthesis and modification of nanostructured material and surfaces.

Lars Hultman received the Ph.D. in material science in 1988 from IFM, Linköping University, Linköping, Sweden.

He was a Postdoctoral Fellow with the Northwestern University, Evanston, IL, in 1989–1990. He was a Visiting Professor at the University of Illinois at Urbana–Champaign, Urbana, during 2004–06. He is currently with Linköping University as Full Professor and Division Head of the Thin Film Physics Division. He directs the Center-of-Excellence programs on material science and nanotechnology of functional thin films funded by the Swedish Government, VR, SSF, VINNOVA, and EU-ERC (Advanced Research Grant Awardee), respectively. He has produced 400 papers and is an ISI Most cited researcher. He is also Editor of *Vacuum*.

Prof. Hultman was the recipient of the IUVSTA-Welch Scholarship Award, the Swedish Government award for most prominent young researcher, and the Jacob Wallenberg Foundation Award for Materials Science. He was announced Excellent Researcher by the Swedish Research Council in 2003. He was a fellow of the AVS, fellow of the Forschungszentrum Dresden-Rossendorf, and elected member of the Royal Swedish Academies of Science KVA and IVA.